

APPLICATION OF THE NUCLEAR MATTER APPROACH TO THE INTERACTION POTENTIAL BETWEEN HEAVY IONS*

J. DĄBROWSKI^a, H.S. KÖHLER^b AND J. ROŻYNEK^a

^aTheoretical Division, A. Sołtan Institute for Nuclear Studies
Hoża 69, 00-681 Warsaw, Poland

^bUniversity of Arizona, Tucson, AZ 85721, USA

(Received May 15, 2003)

A simple theory of the interaction potential between heavy ions \mathcal{V} , based on the local density approach and the frozen density model, is applied to a number of pairs of nuclei with neutron excess. The energy density needed for calculating \mathcal{V} is expressed in a simple way through the equilibrium properties of nuclear matter, a phenomenological density gradient term, and nucleon density distributions in the two colliding nuclei. The Coulomb barrier in the calculated potential compares favorably with other estimates.

PACS numbers: 25.70.-z

1. Introduction

The theoretical description of heavy ion collisions requires the knowledge of the interaction potential \mathcal{V} between the two colliding ions. A simple nuclear matter (NM) approach to \mathcal{V} was presented in [1] (hereafter referred to as I). It was an extension of our previous work Refs [2–5] restricted to equal number of neutrons and protons, $N = Z$, to the case of ions with neutron excess, $N > Z$. Our approach allows to determine \mathcal{V} directly from the known properties of NM¹. The input of our simple calculations consists of: equilibrium density, volume and symmetry energy of NM, nucleon effective mass in NM, empirical densities in the colliding nuclei, and a phenomenological density gradient correction to the energy density.

* This research was partly supported by the Polish State Committee for Scientific Research (KBN) under grant No. 2P03B7522 and the National Science Foundation under grant No. PHY-0070828.

¹ In a simplified form, the approach was applied a long time ago by Brueckner *et al.* [6] (see also [7]).

In the present paper, we apply the scheme of I to describe the scattering of a number of heavy ions. The paper is organized as follows. In Sec. 2, the main results of I are summarized. In Sec. 3 the results obtained for \mathcal{V} for a number of heavy ions are presented and discussed.

2. The nuclear matter approach to \mathcal{V}

We consider nuclei 1 (target) and 2 (projectile) (with masses M_1, M_2 , and with the reduced mass $\mu = M_1 M_2 / (M_1 + M_2)$), moving with relative momentum \mathbf{K}_{REL} (in units of \hbar). We denote by \mathbf{R} the relative position vector between the centers of mass of 1 and 2 (directed from 1 to 2). In the CM system \mathcal{V} is defined by the relation

$$\mathcal{V}(E, R) = \mathcal{E}_{\text{CM}}(K_{\text{REL}}, R) - \frac{\hbar^2 K_{\text{REL}}^2}{2\mu} - \mathcal{E}_{\text{in}}(1) - \mathcal{E}_{\text{in}}(2), \quad (1)$$

where $\mathcal{E}_{\text{in}}(i)$ is the intrinsic nuclear energy of the isolated nucleus i and \mathcal{E}_{CM} is the nuclear energy of the total system in the CM frame.

The conservation of the total energy implies that the instantaneous relative momentum $\mathbf{K}_{\text{REL}} = \mathbf{K}_{\text{REL}}(R)$ is changing with R

$$\frac{\hbar^2 K_{\text{REL}}(R)^2}{2\mu} + \mathcal{V}(E, R) + \mathcal{V}_{\text{C}}(R) = \frac{\hbar^2 K_{\text{REL}}(\infty)^2}{2\mu} = E, \quad (2)$$

where $\mathcal{V}_{\text{C}}(R)$ is the Coulomb potential between nuclei 1 and 2, and E is the CMS kinetic energy.

The two main ingredients of the approach of I to the problem of calculating $\mathcal{E}_{\text{CM}}(K_{\text{REL}}, R)$ are the local density approximation and the frozen density model.

According to the local density approximation, for a given distance R the system of the two colliding nuclei is approximated locally (at each point \mathbf{r}) by a piece of nuclear matter (NM) with the neutron and proton densities ρ_n and ρ_p , and with the corresponding momentum distributions $n_n(\mathbf{k}_n)$ and $n_p(\mathbf{k}_p)$. If we denote by $H_{\text{CM}}^{\text{NM}}$ the energy density of this local NM in the CM frame, we have

$$\mathcal{E}_{\text{CM}}(K_{\text{REL}}, R) = \int d\mathbf{r} H_{\text{CM}}^{\text{NM}}(K_{\text{REL}}, R; \mathbf{r}). \quad (3)$$

To determine the densities and momentum distributions, we apply the frozen density model (the sudden approximation), in which

$$\rho_y(\mathbf{r}) = \rho_{1y}(r) + \rho_{2y}(|\mathbf{r} - \mathbf{R}|), \quad (4)$$

where ρ_{iy} ($y = n, p; i = 1, 2$) are the original neutron and proton densities of nuclei 1 and 2. (The origin of \mathbf{r} and \mathbf{R} is the center of 1.) For the local momentum distributions of neutrons (protons) in nucleus 1 and 2 at \mathbf{r} we have two Fermi spheres $10n(p)$ and $20n(p)$ with the respective local Fermi momenta

$$k_{F10y}(r) = [3\pi^2\rho_{1y}(r)]^{1/3}, \quad k_{F20y}(\mathbf{r}) = [3\pi^2\rho_{2y}(|\mathbf{r} - \mathbf{R}|)]^{1/3}, \quad (5)$$

with the center of the Fermi sphere 2 shifted from the center of the Fermi sphere 1 by \mathbf{K}_r , (twice) the average relative nucleon momenta in nucleus 2 and nucleus 1,

$$\mathbf{K}_r = \left(\frac{m}{\mu}\right) \mathbf{K}_{\text{REL}}, \quad (6)$$

where m is the nucleon mass.

When $K_r < k_{F10y} + k_{F20y}$, the two Fermi spheres $10y$ and $20y$ overlap, and we face the problem of the double occupancy in the overlap region. We resolve this problem by increasing $k_{F10y} \rightarrow k_{F1y}$ and $k_{F20y} \rightarrow k_{F2y}$, and obtain our final momentum distributions with the Fermi surfaces $1y$ and $2y$ with the increased Fermi momenta and with a single occupancy in the overlap region. Details of this reshuffling of neutrons and protons from the original distributions (with the double occupancy in the overlap region) to our final distributions are presented in I. This reshuffling, *i.e.* determination of k_{F1y} and k_{F2y} , was accomplished with a numerical procedure.

To calculate the energy density of the local NM, we go over to the rest frame of the local NM. Our NM energy density H^{NM} in this frame differs from H_0^{NM} , the energy density of normal NM (*i.e.*, NM in its ground state) with the same neutron and proton densities by the two-sphere momentum distributions of neutrons and protons, which in normal NM are single Fermi spheres. To change normal NM into our local NM one has to redistribute neutrons and protons from their single Fermi sphere distributions into the two-sphere distributions. The corresponding change in the energy density is determined by the single particle (s.p.) energies of the states involved in the redistribution. In this way we get

$$H^{\text{NM}} = f(\rho, \alpha)\rho + \frac{1}{v}(\tau_n + \tau_p - \tau_{0n} - \tau_{0p}), \quad (7)$$

where ρ is the total local density, $\alpha = (\rho_n - \rho_p)/\rho$ is the neutron excess parameter, and τ_y and τ_{0y} are the kinetic energy densities (in the rest frame of NM) in our local NM and in normal NM². The second part on the r.h.s. of Eq. (7) represents the change in the energy density caused by the redistribution of nucleons in momentum space. Here we assume for the s.p.

² Whereas for τ_{0y} we have simple expressions, $\tau_{0y} = \frac{3}{5}\varepsilon(k_{Fy})\rho_y$, also for τ_y we have (slightly longer) analytical expressions.

energies the effective mass approximation with the ratio of the effective to the real nucleon mass by $m^*/m = \nu = \nu(\rho)$.

The first term on the r.h.s. of Eq. (7) is the energy density of normal NM, $f(\rho, \alpha)\rho = H_0^{\text{NM}} = (E_0^{\text{NM}}/A)\rho$. We expand $f(\rho, \alpha)$, the energy per nucleon in normal nuclear matter, in powers of α

$$f(\rho, \alpha) = f_0(\rho) + \frac{1}{2}\alpha^2 \varepsilon_{\text{sym}}(\rho). \quad (8)$$

For f_0 , we assume the form

$$f_0(\rho) = \frac{3}{5}\varepsilon(k_{\text{F}}) + \sum_{j=3}^5 a_j \left(\frac{k_{\text{F}}}{k_{\text{F}0}}\right)^j, \quad (9)$$

where $\varepsilon(k) = \hbar^2 k^2/2m$, $k_{\text{F}} = (3\pi^2\rho/2)^{1/3}$ is the Fermi momentum of normal NM with $N = Z$ and $k_{\text{F}0}$ is the value of k_{F} at equilibrium density ρ_0 . The coefficients a_j are determined by $k_{\text{F}0}$, by the volume energy of NM, $\varepsilon_{\text{vol}} = f_0(\rho_0)$, and by the compressibility $K_c = k_{\text{F}0}^2(d^2 f_0/dk_{\text{F}}^2)_{k_{\text{F}0}}$.

The nuclear symmetry energy at density ρ , $\varepsilon_{\text{sym}}(\rho)$ is connected with the Lane [8] potential V_1 ³

$$\varepsilon_{\text{sym}}(\rho) = \frac{2}{3}\frac{\varepsilon(k_{\text{F}})}{\nu(\rho)} + \frac{1}{4}V_1(\rho). \quad (10)$$

This relation allows us to write H^{NM} in the form

$$H^{\text{NM}} = f_0(\rho)\rho + \frac{1}{\nu}(\tau_n + \tau_p - \tau_0) + \frac{1}{2}\alpha^2\frac{1}{4}V_1\rho, \quad (11)$$

where $\tau_0 = \frac{3}{5}\varepsilon(k_{\text{F}})\rho$ is the kinetic energy density in normal NM with $N = Z$.

We assume that the Lane potential is proportional to the density of NM

$$V_1(\rho) = \frac{\rho}{\rho_0} V_1(\rho_0). \quad (12)$$

For the dependence of ν on ρ , we use the relation

$$\frac{1/\nu(\rho) - 1}{1/\nu_0 - 1} = \frac{\rho}{\rho_0}, \quad (13)$$

where $\nu_0 = \nu(\rho_0)$.

In conclusion, the form of the energy density H^{NM} is specified if we fix the values of ρ_0 (or $k_{\text{F}0}$), ε_{vol} , K_c , $\varepsilon_{\text{sym}}(\rho_0) \equiv \varepsilon_{\text{sym}}$ (or $V_1(\rho_0)$), and ν_0 .

³ The contribution of the Lane potential to the neutron/proton s.p. potential is (+/-) $\frac{1}{4}\alpha V_1$.

When we go back to the CM frame and apply definition (1) of \mathcal{V} , we get

$$\mathcal{V}(E, R) = \int d\mathbf{r} \left\{ H^{\text{NM}} + H_{\nabla} - \frac{\hbar^2 K_r^2}{2m} \frac{\rho_1 \rho_2}{\rho} \right\} - \mathcal{E}_{\text{in}}(1) - \mathcal{E}_{\text{in}}(2). \quad (14)$$

In (14) we go beyond the local density approximation and following Brueckner *et al.* [9] we introduce the gradient correction term

$$H_{\nabla} = H_{\nabla}(\rho) = \frac{\eta_{\text{W}}(\nabla\rho)^2}{\rho} + \eta_{\text{V}}(\nabla\rho)^2, \quad (15)$$

where $\eta_{\text{W}} = \hbar^2/72m$. The first term in (15) is the Weizsäcker correction to the kinetic energy density, and the second one is the gradient correction to the potential energy density, in which η_{V} is treated as a phenomenological parameter.

In calculating the intrinsic energies $\mathcal{E}_{\text{in}}(i)$ we apply the expression

$$\mathcal{E}_{\text{in}}(i) = \int d\mathbf{r} \{ f(\rho_i, \alpha_i) \rho_i + H_{\nabla}(\rho_i) \}, \quad (16)$$

where $\alpha_i = (\rho_{\text{in}} - \rho_{\text{ip}})/\rho_i$.

3. Results and discussion

For a given CM energy E , we know only $K_{\text{REL}}(\infty) = (2\mu E)^{1/2}/\hbar$, whereas expression (14) for $\mathcal{V}(E, R)$ depends on $K_{\text{REL}} = K_{\text{REL}}(R)$ connected with $K_{\text{REL}}(\infty)$ by energy conservation Eq. (2) which in turn contains $\mathcal{V}(E, R)$. We solve this problem by iteration which we start by calculating $\mathcal{V}^{(0)}$ with the help of expression (14) with $K_{\text{REL}} = K_{\text{REL}}(\infty)$. In the next step, we calculate $\mathcal{V}^{(1)}$ by applying expression (14) with $K_{\text{REL}} = K_{\text{REL}}^{(0)}(R)$, obtained from Eq. (2) with $\mathcal{V} = \mathcal{V}^{(0)}$. After a few steps, we obtain $\mathcal{V}^{(i)} = \mathcal{V}^{(i-1)} = \mathcal{V}$.

For the \mathbf{r} -integration in (14) we use cylindrical coordinates with the z -axis along \mathbf{R} . We assume that \mathbf{K}_r is parallel to \mathbf{R} , which reduces the \mathbf{r} -integration to a twofold integration, performed by means of the Gauss formula.

To obtain the Coulomb energy \mathcal{E}_{C} of a nucleus, we approximate the charge distribution in this nucleus by the equivalent uniform charge distribution of radius $R_{\text{C}} = [5\langle r^2 \rangle/3]^{1/2}$, and use the expression $\mathcal{E}_{\text{C}} = 3Z^2 e^2/5R_{\text{C}}$. Similarly, to obtain the Coulomb interaction $\mathcal{V}_{\text{C}}(R)$, we approximate charge distributions in nuclei 1 and 2 by equivalent uniform charge distributions and calculate $\mathcal{V}_{\text{C}}(R)$ as the Coulomb interaction between these two uniform charge distributions.

If we do not state otherwise, we use the following standard parameters of normal NM: $k_{F0} = 1.35 \text{ fm}^{-1}$ ($\rho_0 = 0.166 \text{ fm}^{-3}$), $\varepsilon_{\text{vol}} = -15.8 \text{ MeV}$, $K_c = 234.9 \text{ MeV}$ [$a_5 = 0$ in (9)], $V_1(\rho_0) = 100 \text{ MeV}$ ($\varepsilon_{\text{sym}} = 61.0 \text{ MeV}$), and $\nu_0 = 0.7$.

For the nucleon density distributions, we use two- and three-parameter Fermi models (2pF and 3pF) and three-parameter Gaussian model (3pG) with parameters taken from Refs [11,12]. In the present paper we assume the same radial shape of the neutron and proton density distributions.

The value of the phenomenological parameter $\eta = 22 \text{ MeV fm}^5$ was adjusted to the ground state energies $\mathcal{E} = \mathcal{E}_{\text{in}} + \mathcal{E}_{\text{C}}$ [with the intrinsic nuclear energy \mathcal{E}_{in} calculated according to Eq. (16)] of ^{16}O and ^{40}Ca .

Values of the parameters of the density distribution of nuclei considered in the present paper are presented in Table I which also contains values of the calculated root-mean square radii $\langle r^2 \rangle^{1/2}$. Furthermore, we also present in Table I the calculated values of \mathcal{E} together with their experimental values \mathcal{E}_{exp} . We notice a satisfying agreement between these two values.

In our discussion we shall present our results for the nuclear potential \mathcal{V} , and for $\mathcal{V}_{\text{tot}}(E, R) = \mathcal{V}(E, R) + \mathcal{V}_{\text{C}}(R)$ for different values of $K_r = K_r(\infty)$. The connection between E_{LAB}/A_2 (the kinetic energy in the LAB system of the projectile nucleus 2 per projectile nucleon) and K_r (in fm^{-1}) is

$$\frac{E_{\text{LAB}}}{A_2} = \frac{\hbar^2 K_r^2}{2m} = 20.7 K_r^2 \text{ MeV}. \quad (17)$$

TABLE I

Parameters of the density distributions and values of the ground state energies and their experimental values. All lengths are in fm and energies in MeV.

Nucl.	Model	c	z	w	$\langle r^2 \rangle^{1/2}$	\mathcal{E}_{cal}	$\mathcal{E}_{\text{exp}}^{\text{a}}$
^{40}Ca	3pF ^b	3.766	0.586	-0.161	3.482	-341.9	-342.1
^{48}Ca	3pF ^b	3.7369	0.5245	-0.030	3.469	-428.3	-416.0
^{90}Zr	3pG ^b	4.434	2.528	0.350	4.274	-778.6	-783.9
^{208}Pb	3pF ^c	6.504	0.552743	0.14	5.511	-1640.4	-1636.4
^{238}U	2pF ^b	6.8054	0.6054	0.	5.740	-1794.8	-1801.7

^aTaken from Ref. [10].

^bParameters taken from Ref. [11].

^cParameters taken from Ref. [12].

For the CMS kinetic energy E , we have

$$E = \frac{\mu}{m} \hbar^2 \frac{K_r^2}{2m} = 20.7 \frac{\mu}{m} K_r^2 \text{ MeV}. \quad (18)$$

Let us consider as an example the case of the potential between ^{208}Pb (target) and ^{48}Ca (projectile) nuclei. Results obtained in this case for \mathcal{V} and $\mathcal{V}_{\text{tot}} = \mathcal{V} + \mathcal{V}_C$ for a number of K_r values between 0 and 2.5 fm^{-1} are shown in Fig. 1.

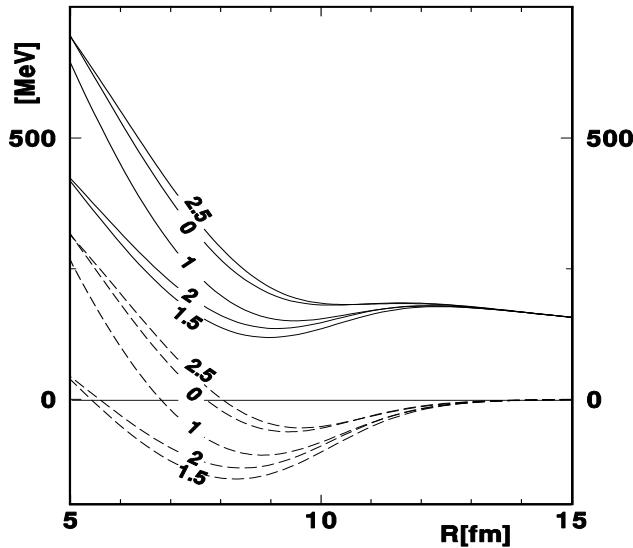


Fig. 1. Potentials \mathcal{V} (broken curves) and \mathcal{V}_{tot} (solid curves) between ^{208}Pb and ^{48}Ca nuclei at the indicated values (in fm^{-1}) of K_r .

The most striking feature of our results is the dependence of \mathcal{V} on $K_r(\infty)$, *i.e.* on the energy E , and the R -dependence of \mathcal{V} : short range repulsion⁴ + long range attraction. A detailed discussion of this behavior of \mathcal{V} in case of $N = Z$ presented in [2] and [3] applies also to the present case. Here, we recall briefly the main points of our previous discussion.

The dependence of \mathcal{V} on K_r is non-monotonic. At small values of K_r , \mathcal{V} decreases (algebraically, *i.e.* becomes more attractive) up to $K_r \approx 1.5 \text{ fm}^{-1}$. If we further increase K_r , \mathcal{V} starts to increase and eventually becomes partly repulsive. Let us recall that at small values of K_r , we increase the radii of the two Fermi spheres in our momentum distributions to avoid double occupancy in the overlap region, which would violate the exclusion principle. This leads to an increase in the kinetic energy, which gives a repulsive contribution to \mathcal{V} .

⁴ For lighter ions instead of the short range repulsion we may have a weakened attraction (see *e.g.* [3, 4]).

This Pauli blocking effect becomes less important when K_r increases, which explains the initial decrease in \mathcal{V} . On the other hand, the potential energy contribution to \mathcal{V} increases (algebraically) with increasing K_r , which may be traced back to the short range NN repulsion. This explains the increase in \mathcal{V} at larger values of K_r .

To explain the dependence of \mathcal{V} on R , let us notice that at small (large) values of R , a substantial part of the combined system has a density $\rho > \rho_0$ ($\rho < \rho_0$). Hence at an intermediate distance R , a substantial part of the combined system has a density $\rho \approx \rho_0$, at which the density of normal NM attains its minimum. Consequently at an intermediate distance \mathcal{V} in the static limit ($K_r = 0$) attains a minimum. For $K_r \neq 0$ the repulsive Pauli blocking effect is weakened especially at large distances R , *i.e.* small densities, and thus the repulsion is shifted towards small distances R .

When we add to \mathcal{V} the Coulomb potential \mathcal{V}_C , we obtain the total potential \mathcal{V}_{tot} which also is nonmonotonic. It contains a Coulomb barrier and a dip inside of the barrier. Whereas the height (~ 180 MeV) and position ($R \sim 12$ fm) of the barrier depends only weakly on K_r the depth of the dip (~ 59 MeV at $K_r = 1.5$ MeV, and ~ 2 MeV at $K_r = 2.5$ MeV) and its location are quite sensitive to the magnitude of K_r .

All the curves in Fig. 1 (as well as in all remaining figures) were obtained with the R dependent $K_r(R)$ except for the case $K_r = 0$ in which we used $K_r(R) = K_r(\infty) = 0$. This case of the static limit corresponds exactly to the model applied in the pioneering paper of Brueckner *et al.* [6].

The sensitivity of our results for \mathcal{V} to the magnitude of the Lane potential V_1 (or equivalently to the symmetry energy ε_{sym}) is visualized in Fig. 2, where we show results for the $^{208}\text{Pb}-^{48}\text{Ca}$ potential at $K_r = 1.5 \text{ fm}^{-1}$ obtained with $V_1 = 100$ MeV ($\varepsilon^{\text{sym}} = 61.0$ MeV) and with $V_1 = 0$ ($\varepsilon^{\text{sym}} = 36.0$ MeV), with all the remaining parameters unchanged. We also consider the case in which we artificially assume that there is no neutron excess in both nuclei ^{208}Pb and ^{48}Ca , *i.e.* we replace Z_i and N_i ($i = 1, 2$) by $A_i/2$ (but use the real Z_i values in calculating Coulomb energies) and use the same $3pF$ density distributions. The corresponding curves in Fig. 1 are marked as “ $\alpha = 0$ ”. We notice that taking into account the neutron excess, and increasing the Lane potential (or equivalently the symmetry energy) increases both \mathcal{V} and \mathcal{V}_{tot} , although the height of the Coulomb barrier remains practically unchanged.

The behavior of \mathcal{V} and \mathcal{V}_{tot} at $K_r = 1.5 \text{ fm}^{-1}$ for a selection of pairs of nuclei is shown in Fig. 3. The height B of the Coulomb barrier for these pairs of nuclei are presented in Table II together with other estimates of B : results of the Hartree-Fock calculations of Skalski [13], the estimates of the fusion threshold barriers B_{thre} by Siwek-Wilczyńska and Wilczyński [15], and Bass [14] interaction barriers B_{int} . We see that our results agree very nicely with the other results.

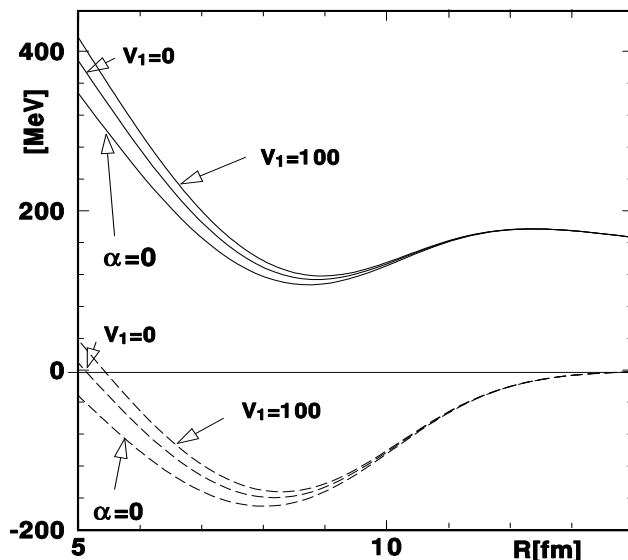


Fig. 2. Potentials \mathcal{V} (broken curves) and \mathcal{V}_{tot} (solid curves) between ^{208}Pb and ^{48}Ca at $K_r = 1.5 \text{ fm}^{-1}$ for $V_1 = 100 \text{ MeV}$, and $V_1 = 0$. The $\alpha=0$ curves were obtained by disregarding the neutron exes.

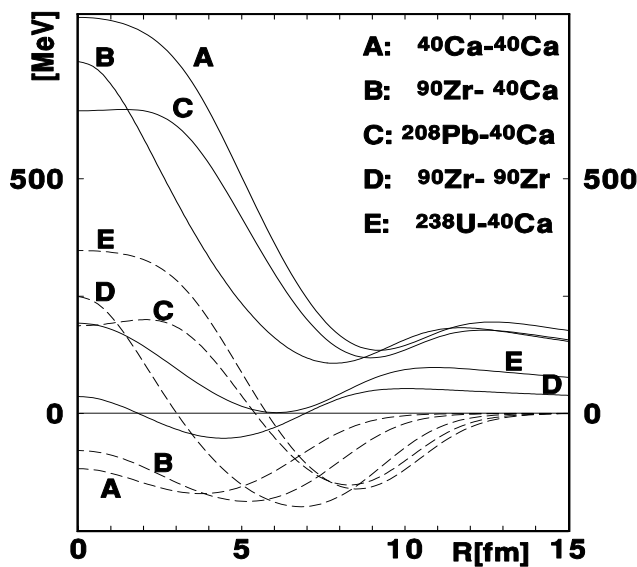


Fig. 3. Potentials \mathcal{V} (broken curves) and \mathcal{V}_{tot} (solid curves) between the indicated pairs of nuclei at $K_r = 1.5 \text{ fm}^{-1}$.

TABLE II

Results of the present work for the Coulomb barrier B in MeV at $K_r = 1.5 \text{ fm}^{-1}$ compared with other estimates.

Nuclei	$B_{\text{pres.work}}$	B^{a}	B_{thre}	$B_{\text{int}}^{\text{b}}$
$^{40}\text{Ca}-^{40}\text{Ca}$	52.7	53	$50.2 \pm 0.2^{\text{c}}$	52.54
$^{90}\text{Zr}-^{40}\text{Ca}$	97.8	95	$92.7 \pm 0.6^{\text{c}}$	97.7
$^{208}\text{Pb}-^{48}\text{Ca}$	177.3	173.5	$169 \pm 2^{\text{c}}$	176.1
$^{90}\text{Zr}-^{90}\text{Zr}$	183.4	180	$\sim 175.85^{\text{d}}$	181.0
$^{238}\text{U}-^{48}\text{Ca}$	194.8	174.5(191)	$182 \pm 2^{\text{c}}$	193.8

^aCalculated in Ref. [13].

^bInteraction barriers of Ref. [14].

^cThreshold barrier estimated in Ref. [15].

^dThreshold barrier estimated in Ref. [13].

We use the frozen density model, and a rough criterion for its applicability is that E_{LAB}/A_2 should be larger than the intrinsic kinetic energy per nucleon in the colliding nuclei, *i.e.*, about 30 MeV. This implies the condition $K_r = K_r(\infty) \gtrsim 1.2 \text{ fm}^{-1}$ [see Eq. (17)]⁵. Thus in principle, we should not apply our approach to the very small values of K_r which correspond to $E \sim B$, *i.e.* to threshold energies determined in [15] and to the energies applied in [14] in determining B_{int} , or to the static limit $E \rightarrow 0$ applied in [13]. Nevertheless the favorable comparison of our results for B with the theoretical results of [13] and the estimates of the threshold barriers of [15], and with B_{int} [14] appears meaningful because of the weak dependence on K_r of our results for B . Notice that the Coulomb barrier attains its maximum at distances R at which only the tails of the densities of the colliding nuclei overlap.

The interesting behavior of \mathcal{V} at smaller distances R shown in Fig. 3 is hard to test experimentally, because strong absorption⁶ and also Coulomb repulsion make the region of small distances practically inaccessible in the elastic channel. (For this reason the range of smallest distances R is not shown in Figs. 1 and 2.)

⁵ On the other hand, an upper limit on K_r is imposed by our use of nonrelativistic theory: for $K_r = 3.4 \text{ fm}^{-1}$, we already have $E_{\text{LAB}}/A_2 \cong \frac{1}{4}mc^2$. Also approximation (7) puts an upper limit on K_r .

⁶ See *e.g.* Refs [3, 4].

The authors are obliged to Janusz Skalski for his illuminating comments concerning the fusion barrier, and for letting us know his results prior to publication.

REFERENCES

- [1] J. Dąbrowski, H.S. Köhler, *Acta Phys. Pol. B* **34**, 1987 (2003).
- [2] J. Dąbrowski, H.S. Köhler, *Nucl. Phys.* **A489**, 303 (1988).
- [3] J. Dąbrowski, H.S. Köhler, *Nucl. Phys.* **A499**, 413 (1989).
- [4] J. Dąbrowski, *Acta Phys. Pol. B* **20**, 61 (1989).
- [5] J. Dąbrowski, *Acta Phys. Pol. B* **21**, 223 (1990); *Phys. Lett.* **B240**, 33 (1990).
- [6] K.A. Brueckner, J.R. Buchler, M.M. Kelly, *Phys. Rev.* **173**, 944 (1968).
- [7] F. Beck, K.-H. Mueller, H.S. Köhler, *Phys. Rev. Lett.* **40**, 837 (1978).
- [8] A.M. Lane, *Nucl. Phys.* **A128**, 256 (1969).
- [9] K.A. Brueckner, J.R. Buchler, S. Jorna, R.J. Lombard, *Phys. Rev.* **171**, 1188 (1968).
- [10] G. Audi, A.H. Wapstra, *Nucl. Phys.* **A595**, 409 (1995).
- [11] H. de Vries *et al.*, *At. Data Nucl. Data Tables* **36**, 495 (1987).
- [12] R. Engfer *et al.*, *At. Data Nucl. Data Tables* **14**, 509 (1974).
- [13] J. Skalski, *Acta Phys. Pol. B* **34**, 1977 (2003).
- [14] R. Bass, *Nucl. Phys.* **A231**, 45 (1974).
- [15] K. Siwek-Wilczyńska, J. Wilczyński, *Phys. Rev.* **C64**, 024611 (2001).